Pharmacokinetic Modeling and Biodistribution Estimation Through the Molecular Communication Paradigm

Youssef Chahibi*, *Student Member, IEEE*, Massimiliano Pierobon, *Member, IEEE*, and Ian F. Akyildiz, *Fellow, IEEE*

***Abstract*—Targeted drug delivery systems (TDDSs) are therapeutic methods based on the injection and delivery of drug-loaded particles. The engineering of TDDSs must take into account both the therapeutic effects of the drug at the target delivery location and the toxicity of the drug while it accumulates in other regions of the body. These characteristics are directly related to how the drug-loaded particles distribute within the body, i.e., biodistribution, as a consequence of the processes involved in the particle propagation, i.e., pharmacokinetics. In this paper, the pharmacokinetics of TDDSs is analytically modeled through the abstraction of molecular communication, a novel paradigm in communication theory. Not only is the particle advection and diffusion, considered in our previous study, included in this model, but also are other physicochemical processes in the particle propagation, such as absorption, reaction, and adhesion. In addition, the proposed model includes the impact of cardiovascular diseases, such as arteriosclerosis and tumor-induced blood vessel leakage. Based on this model, the biodistribution at the delivery location is estimated through communication engineering metrics, such as channel delay and path loss, together with the drug accumulation in the rest of the body. The proposed pharmacokinetic model is validated against multiphysics finite-element simulations, and numerical results are provided for the biodistribution estimation in different scenarios. Finally, based on the proposed model, a procedure to optimize the drug injection rate is proposed to achieve a desired drug delivery rate. The outcome of this study is a multiscale physics-based analytical pharmacokinetic model.**

***Index Terms*—Biodistribution, inverse problem, molecular communication, nanonetworks, pharmacokinetics, targeted drug delivery systems.**

I. Introduction

TARGETED drug delivery systems (TDDSs) [1] are cutting-edge therapeutic methods, which aim at delivering the drug exactly where it is needed while minimizing the adverse effects of the drug on the other healthy parts of the body, by using micro or nanosized drug-loaded particles. The estimation of how the drug-loaded particles distribute within the body, named biodistribution, is essential for TDDS engineering, and it is directly related to the processes involved in the particle propagation, such as their advection and diffusion in the blood stream, their absorption from surrounding tissues, and their chemical and physical interactions with other biomolecules present in the body. Although drug biodistribution can be estimated empirically through clinical experiments, these are rarely performed because of the ethical and financial constraints they pose [2] and their specificity to each individual subject.

Recent advances in biomaterials allow the engineering of drug particles with very specific chemical and geometric properties in order to provide a targeted drug delivery. To benefit from these technological advances and study the properties of drug particles to guarantee an optimal biodistribution, the aforementioned particle propagation processes have to be modeled through the study of the so-called drug pharmacokinetics. The most successful existing TDDS pharmacokinetic models are based on the multicompartmental approach [3], where large portions of the human body are considered as single compartments, with homogeneous chemical and physical properties. The pharmacokinetics in one compartment is commonly described through first-order differential equations, and the evolution of the pharmacokinetics is obtained for a time scale in the order of hours. These models include: 1) Target-mediated drug disposition [4], where the equations are based on a very limited number of parameters that are empirically derived; 2) PK/PD (pharmacokinetics and pharmacodynamics) [5], where the equation parameters are statistically derived from experimental work, and the pharmacokinetics is modeled only locally within a spatial scale of a cell; 3) PBPK (physiologically-based pharmacokinetics) [6], where pharmacokinetics is modeled globally for the whole body but by considering each organ as a single compartment where the drug is homogeneously distributed.

Especially, nanomedicine-enabled TDDSs require new pharmacokinetic models where the particle propagation processes within the body are described in greater precision at a much smaller time and space resolution, and in a tractable manner, whereas the aforementioned models account for particle propagation only at the spatial resolution of organs and the time scale of days. Moreover, the existing models are not sufficiently scalable and are not customizable to the patients and their specific diseases [3].

To tackle the aforementioned problems, we propose a TDDS pharmacokinetic model based on the abstraction of molecular communication (MC), a recently developed paradigm in

Manuscript received January 17, 2014; revised April 23, 2015; accepted April 25, 2015. Date of publication May 6, 2015; date of current version September 16, 2015. This work was supported in part by the Samsung Advanced Institute of Technology, Global Research Outreach Program, under project title: Molecular Communication Fundamentals in Action Potential-Triggered Targeted Drug Delivery Systems, and the US National Science Foundation under Grant MCB-1449014. *Asterisk indicates corresponding author*

*Y. Chahibi is with the Broadband Wireless Networking Laboratory, School of Electrical and Computer Engineering, Georgia Institute of Technology, Atlanta, GA 30332 USA (e-mail: youssef@ece.gatech.edu).

M. Pierobon is with the University of Nebraska-Lincoln.

I. F. Akyildiz is with the Georgia Institute of Technology.

Color versions of one or more of the figures in this paper are available online at http://ieeexplore.ieee.org.

Digital Object Identifier 10.1109/TBME.2015.2430011

communication theory that defines information exchange through the emission, propagation, and reception of molecules. In [7], we developed an MC model to calculate the time-varying blood velocity in any location of the cardiovascular system, and to predict the propagation of the drug-loaded particles due to advection and diffusion in the blood flow. In this paper, by stemming from our previous work, we develop a TDDS pharmacokinetic model able to predict the propagation of the particles by taking into account other specific physicochemical processes, as well as abnormal health conditions. Through the MC paradigm, we consider the following physicochemical processes:

1) The *advection process*, which represents the transport of particles due to the blood velocity.
2) The *diffusion process*, which corresponds to the Brownian motion of particles.
3) The *absorption process*, which quantifies the particles absorption through tissues surrounding the blood vessels [8].
4) The *reaction process*, which is a consequence of the degradation of particles in the blood [9].
5) The *adhesion process*, which accounts for other biomolecules binding to the drug-loaded particles. The adhesion process is one of the main adverse effects to the performance of the TDDSs [10].

In the proposed pharmacokinetic model, we also account for the effects on the drug pharmacokinetics of cardiovascular diseases, which include blood vessel leakage, e.g., due to tumors, and rigidity, e.g., due to arteriosclerosis. These effects are analytically considered in the proposed pharmacokinetic model, and are shown to greatly affect the drug particle distribution through numerical evaluations of the pharmacokinetic model and the biodistribution estimation.

Compared to the aforementioned existing models, the proposed pharmacokinetic model can be used at different spatial scales (organs, small tissues, and cells) and at a more precise time scale, where the drug pharmacokinetics is predicted within fractions of seconds. Moreover, our model does not require empirically-obtained parameters and it has a lower computational complexity.

By stemming from the proposed MC-based pharmacokinetic model, we propose a method to estimate the drug biodistribution. We propose to characterize the presence of the drug at the delivery location through communication engineering metrics, namely, channel delay and path loss, analytically derived from the proposed pharmacokinetic model. The channel delay corresponds to the time needed by the drug particles to reach their peak concentration at the delivery location after they are injected, while the channel path loss is the ratio of the drug particles that effectively reach the delivery location over the drug particles that were initially injected. In addition, we also demonstrate that the proposed pharmacokinetic model allows to analytically estimate the drug accumulation in the rest of the body.

The proposed MC-based pharmacokinetic model is validated through finite-element simulations on COMSOL, which consider 3-D Navier–Stokes and advection-diffusion-reaction equations to simulate the drug propagation in a time-varying blood flow through a 3-D model of a blood arterial network. The proposed MC-based pharmacokinetic model proves to be in good agreement with the results of the simulation, therefore reproducing similar results with analytical expressions, which do not require the computational complexity of the finite-element simulations. Additionally, numerical results are provided for the biodistribution estimation in different health scenarios, namely, in the presence of arteriosclerosis and tumor-induced blood blood vessel leakage. Through these results, we show that the transport and kinetic properties are important factors influencing the pharmacokinetics of the drug-loaded particles.

Finally, by stemming from the proposed model, we detail a procedure to analytically express the optimal drug injection rate given a target drug delivery rate. For this, we suppose that the healing of the disease requires an objective drug delivery rate, and that the drug injection and delivery locations are known. The proposed pharmacokinetic model is then applied to analytically obtain the optimal drug injection rate.

The rest of the paper is organized as follows. In Section II, we mathematically describe the pharmacokinetic model based on the MC abstraction of the physicochemical processes in the drug-loaded particle propagation, namely, advection, diffusion, reaction, absorption, and adhesion. Moreover, we incorporate in the pharmacokinetic model possible cardiovascular diseases affecting the blood flow. In Section III, we obtain the biodistribution estimation of the particles through the communication engineering metrics of channel path loss and delay, and the expressions to compute the drug accumulation in the rest of the body. Numerical results are provided for the biodistribution in different scenarios. In Section IV, the validation of the MC-based pharmacokinetic model with multiphysics finite element simulation is presented. In Section V, we apply the MC-based pharmacokinetic model to find the optimal drug injection rate that would achieve an objective drug delivery rate at the delivery location. Finally, Section VI concludes the paper with comments about the validity of the model and the various factors influencing the performance of TDDSs.

II. MC-Based Pharmacokinetic Model

In this section, we mathematically describe the pharmacokinetic model of a TDDS based on the analytical MC channel abstraction, which considers additional physicochemical processes in the particle propagation from the injection location to the delivery location, in addition to the advection and diffusion processes already considered in [7].

The network of blood vessels is abstracted here as an MC network. Fig. 1 illustrates the physicochemical processes in a blood network consisting of several blood vessels. $u_n(t)$ denotes the blood velocity in a blood vessel n, and t is the time variable. The drug propagates in this blood network subject to an absorption with rate ρ_n, reaction with rate μ_n, adhesion with an adsorption rate k^+ and a desorption rate k^-, diffusion with a diffusion coefficient D, and advection driven by the blood velocity. The drug propagation is abstracted as an MC

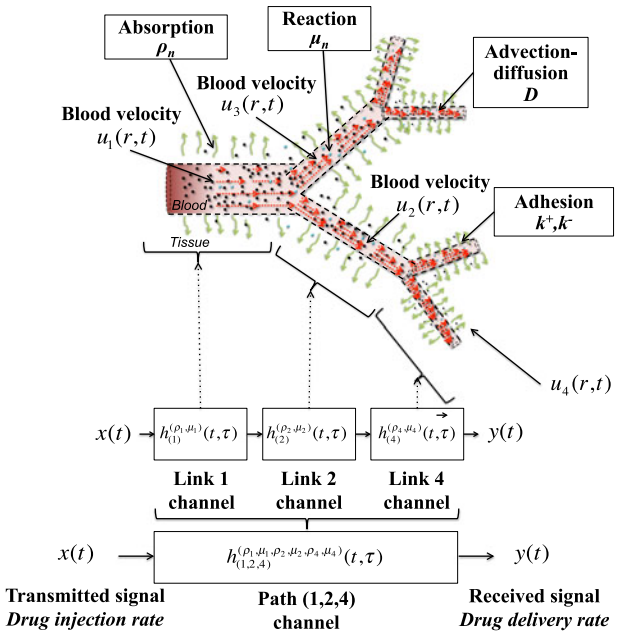

Fig. 1. Scheme of the MC modeling of TDDSs pharmacokinetics.

channel, and completely characterizes the relationship between the drug injection rate and the drug delivery rate. The drug injection rate is the MC signal transmitted at the inlet of the blood vessel and the drug delivery rate is the MC signal received at the outlet of the blood vessel. This is achieved by a time-varying impulse response $h_{(n)}^{(\rho_n,\mu_n)}(t,\tau)$, where τ is a time variable, for every blood vessel n ($n = 1, 2, \ldots, 7$). The MC link channels are cascaded to obtain an MC path, which provides the relationship between the drug injection rate $x(t)$ and the drug delivery rate $y(t)$, through the time-varying impulse response for the path channel, denoted, e.g., by $h_{(1,2,4)}^{(\rho_1,\mu_1,\rho_2,\mu_2,\rho_4,\mu_4)}(t,\tau)$ for the cascade of MC links 1, 2, and 4 as shown in Fig. 1.

In Section II-A, we present how a blood vessel is abstracted as an MC link. In Section II-B, we describe how the physicochemical processes between the drug particles and the body can be modeled by combining MC links. Finally, in Section II-C, the modeling of cardiovascular diseases using equivalent circuits is proposed.

A. MC Link Model

We found in [7] that the drug injection rate $x(t)$ and the drug delivery rate $y(t)$ in the blood vessel n are related mathematically by the following expression:

$$y(t) = \int_{-\infty}^{+\infty} x(\tau) h_{(n)}^{(\rho_n,\mu_n)}(t,\tau) d\tau \,. \tag{1}$$

Due to the fluctuations in the blood flow, the impulse response of the system depends on the state of the blood flow at the time of the injection, therefore the system is not linear time-invariant (LTI). The response of non-LTI systems cannot be expressed in the form of a convolution operation. For the aforementioned reasons, the expression in (1) is different from a convolution. We derive the analytical expression of the time-varying impulse response of the MC link n, as follows:

$$h_{(n)}^{(\rho_n,\mu_n)}(t,\tau) = \frac{\exp\left(-\frac{(l_n - m_n(t,\tau))^2}{2\sigma_n^2(t,\tau)} - \mu_n(t-\tau)\right)}{\sqrt{2\pi\sigma_n^2(t,\tau)}} \tag{2}$$

where:

1) $m_n(t,\tau)$ is a function of *apparent velocity* $v_n(t)$ as follows:

$$m_n(t,\tau) = \int_{\tau}^{t} v_n(t')dt' \tag{3}$$

where t' is the time integration variable.

2) $\sigma_n^2(t,\tau)$ is a function of the *effective diffusivity* $D_n(t)$ as follows:

$$\sigma_n^2(t,\tau) = 2\int_{\tau}^{t} D_n(t')dt' \,. \tag{4}$$

3) μ_n is a characteristic of the *reaction process*, and represents the rate of reaction between the particles and the blood.

In the following, we provide the expression of the apparent velocity $v_n(t)$ and the effective diffusivity $D_n(t)$ for advection-diffusion (see Section II-A1), absorption (see Section II-A2), and adhesion (see Section II-A3).

1) Advection-Diffusion Case (No Reaction): When the reaction process is absent, and only the advection-diffusion is occurring, the *apparent velocity in the case of no reaction* $v_n^{\text{none}}(t)$ and the *effective diffusivity in the case of no reaction* $D_n^{\text{none}}(t)$ are

$$\begin{cases} v_n^{\text{none}}(t) = u_n(t) \\ D_n^{\text{none}}(t) = D + \dfrac{u_n^2(t) r_n^2}{192D} \end{cases} \tag{5}$$

which is a result we derived in [7].

2) Absorption Case: When there is absorption due to the tissues that surround the blood network, the *apparent velocity in the case of absorption* $v_n^{\text{absorption}}(t)$ and the *effective diffusivity in the case of absorption* $D_n^{\text{absorption}}(t)$ are [11]

$$\begin{cases} v_n^{\text{absorption}}(t) = \left(1 + \dfrac{2}{15}\rho_n\right) u_n(t) \\ D_n^{\text{absorption}}(t) = D + \dfrac{{u_n}^2(t) r_n^2}{192D}\left(1 - \dfrac{4}{15}\rho_n\right). \end{cases} \tag{6}$$

3) Adhesion Case: When adhesion to the proteins in the blood plasma or to the blood vessel walls is occurring, the *apparent velocity in the case of adhesion* $v_n^{\text{adhesion}}(t)$ and the

effective diffusivity in the case of adhesion $D_n^{\text{adhesion}}(t)$ are [12]

$$\begin{cases} v_n^{\text{adhesion}}(t) = \dfrac{1}{1+\frac{k^+}{k^-}} u_n(t) \\ D_n^{\text{adhesion}}(t) = \dfrac{r_n^2 u_n^2(t)}{48D} \dfrac{44 r_n^2 \left(\frac{k^+}{k^-}\right)^2 + 12 r_n^2 \frac{k^+}{k^-} + r_n^3}{\left(r_n + 2\frac{k^+}{k^-}\right)^3} \\ \qquad\qquad + \dfrac{2u_n^2(t) r_n^2 \frac{k^+}{k^-}}{k^- \left(r_n + 2\frac{k^+}{k^-}\right)^3}. \end{cases} \tag{7}$$

Section IV-B provides numerical values for the cross-sectional average blood velocities of three blood vessels, obtained using the transmission line method described in [7].

B. MC Path Model

The MC channel model of a path $(n; n = 1 \dots N)$ where n is the index of a link n, is obtained by using the *harmonic transfer matrix* function $\text{HTM}\{\cdot\}$ and its inverse $\text{HTM}^{-1}\{\cdot\}$ [7]

$$y(t) = \int_{-\infty}^{+\infty} x(\tau) h_{(n;n=1\dots N)}^{(\rho_n,\mu_n;n=1\dots N)}(t,\tau) d\tau \tag{8}$$

where the time-varying impulse response of the path $h_{(n;n=1\dots N)}^{(\rho_n,\mu_n;n=1\dots N)}$ is expressed as follows:

$$h_{(n;n=1\dots N)}^{(\rho_n,\mu_n;n=1\dots N)} = \text{HTM}^{-1}\left\{ \prod_{n=N}^{n=1} \text{HTM}\left\{ h_{(n)}^{(\rho_n,\mu_n)}(t,\tau) \right\} \right\}. \tag{9}$$

Through the HTM method [13], we can find analytical solutions of the end-to-end impulse response of TDDSs, as opposed to numerical solutions by finite-element models.

C. Disease Models With Equivalent Circuits

In this section, we present an equivalent circuit modeling of cardiovascular diseases, including arteriosclerosis (rigid blood vessel model), and blood vessel leakage (leaky blood vessel model).

A blood vessel is considered as a cylindrical elastic tube with radius r_n and length l_n, and modeled as an electrical circuit, whose electrical components are related to the geometry of the blood vessels. A healthy blood vessel n possesses three electrical components. First, a resistance R_n, which is related to the blood viscosity and the diameter of the blood vessel. Second, an inductance L_n, which is related to the blood inertia, that is how a difference in blood pressure causes a difference in blood flow. Third, a capacitance C_n, which measures the blood vessel elasticity. We give below the expression of the electrical components based on their physiology [7].

The resistance of the blood vessel n is expressed as follows:

$$R_n = \frac{8\nu}{\pi l_n r_n^4} \tag{10}$$

where ν is the blood viscosity.

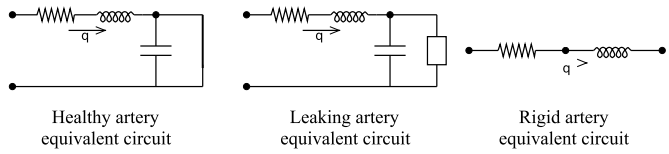

Fig. 2. Equivalent electrical circuits for a blood vessel in different conditions.

The inductance of the blood vessel n is expressed as follows:

$$L_n = \frac{\eta}{\pi l_n r_n^2} \tag{11}$$

where η is the blood density.

1) Rigid Vessel Model: The elasticity of a blood vessel is an important parameter in the success of drug delivery. There have been studies to show how abnormal elasticity affects drug propagation [14]. Blood blood vessels can become rigid because of aging and diseases such as arteriosclerosis [15].

For a rigid blood vessel, we model the change in elasticity using an *arterial elasticity factor*, which measures the ratio between normal elasticity and rigid elasticity. We retain the same electrical components as in the healthy blood vessel model, except for the capacitance, which is now equal to

$$C_n = \frac{\pi {r_n}^2}{F_C(a_1 \exp(-a_2 r_n) + a_3)} \tag{12}$$

where F_C is the arterial elasticity factor ($F_C = 1$ for a healthy blood vessel, $F_C = 0$ for a completely rigid blood vessel). $a_1 = 1.34 \times 10^7 \text{g}/(\text{s}^2 \cdot \text{cm})$, $a_2 = 22.53\ \text{cm}^{-1}$, and $a_3 = 5.77 \times 10^5 \text{g}/(\text{s}^2 \cdot \text{cm})$ are statistical parameters obtained from physiological measurements[16].

2) Leaky Vessel Model: The leakage of a blood vessel is modeled by an equivalent conductance, which is related to how easy it is for a fluid to leak from the blood vessel. We retain the same electrical components as for the healthy blood vessel case, but we add an additional conductance G_n to model the blood vessel leakiness

$$G_n = \frac{F_L}{R_n} \tag{13}$$

where F_L is leakiness factor, which compares the leakage to the conductance of the healthy blood vessel (inverse of the resistance), and R_n is the resistance of the blood vessel.

Fig. 2 shows the equivalent electrical circuit components for a blood vessel in different conditions such as a healthy condition, arteriosclerosis, and blood vessel leakage. By defining electrical equivalents of diseased blood vessels, the blood velocities are calculated by using the transmission line theory method presented in [7], after substituting the expressions of the conductances and the capacitances for healthy blood vessels with the expressions in (12) and (13), respectively. For the numerical results, the inner iliac blood vessel [17] was chosen, and the properties of three of its children blood vessels, denoted as $(3, 6, 7)$ in Figs. 3–5, respectively, have been modified according to the considered disease condition.

In Fig. 3, we observe that in a healthy arterial tree, the blood velocity tends to dampen slowly as we go farther from the root

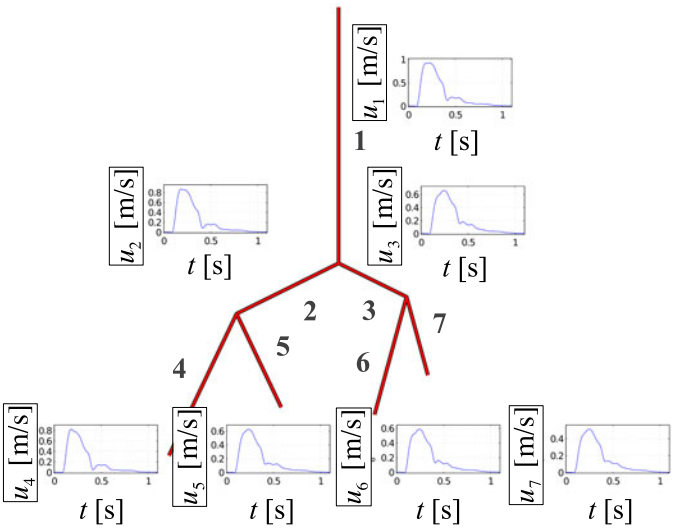

Fig. 3. Blood velocities at a tree of small blood vessels in a healthy condition.

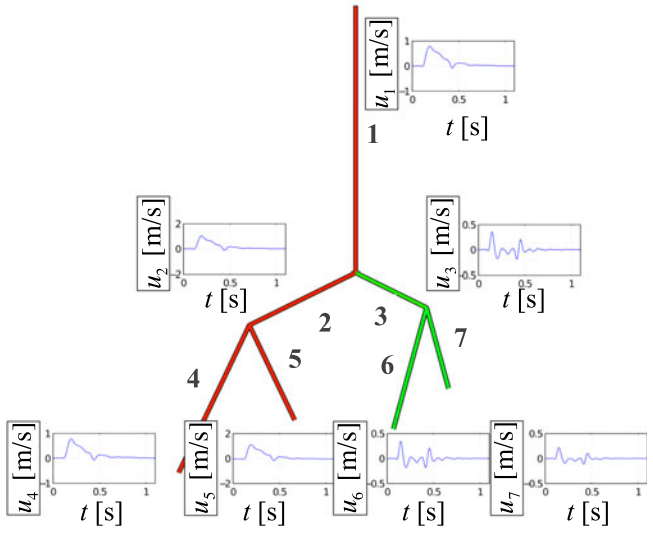

Fig. 5. Blood velocities at a tree of small blood vessels with a branch suffering from arteriosclerosis.

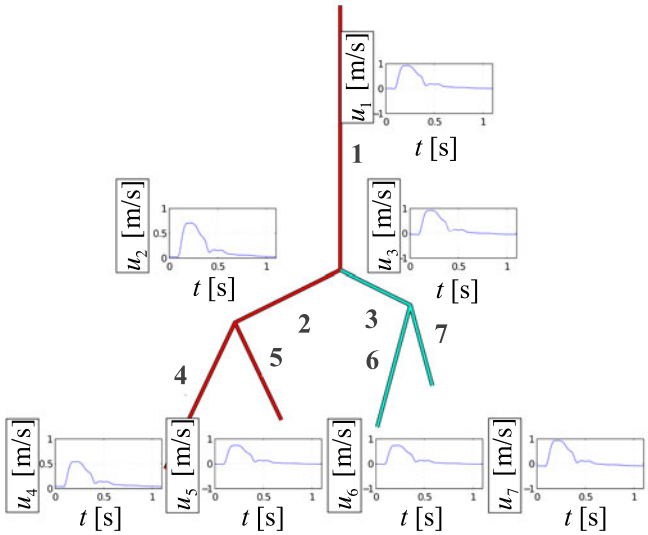

Fig. 4. Blood velocities at a tree of small blood vessels with a branch suffering from blood vessel leakage.

of the blood vessel. In the case of a blood vessel leakage, as illustrated in Fig. 4, this trend is not observed, where we can see that the blood velocity may increase in some daughter blood vessels, since the resistance is reduced. Fig. 5 shows the extreme case where a portion of the arterial tree is affected by a severe arteriosclerosis. In that case, the diseased blood vessels exhibit a highly oscillatory blood flow.

The method introduced in this section can be applied to model the drug propagation in any location of the arterial network.

III. Biodistribution Estimation

The biodistribution is the study of the location and the quantity of the drug that is accumulated in the delivery location and the rest of the body, whether in the blood vessels, their surround tissues, or reacting with elements of the blood plasma. In this section, we estimate the biodistribution of TDDSs using the MC paradigm through the definition of two MC metrics, namely, the channel delay and the channel path loss. In Section III-A, the channel delay is the time needed by the drug particles to reach their peak concentration at the delivery location after they are injected in the body. In Section III-B, the channel path loss is the proportion of the injected particles that reach the delivery location despite the blood vessels branching, reaction, adhesion, and absorption. Finally, in Section III-C, the drug accumulation in the rest of the body is expressed analytically using the MC model.

A. Channel Delay to the Delivery Location

We define the delay for a TDDS as the time required by injected molecules to reach their peak concentration at the delivery location, which is a definition typically used in biodistribution. Another definition of delay used in biodistribution studies is the half-life of a drug [18], which is only meaningful for drugs undergoing an exponential decay. The definition we choose is more general than half-life, and can provide more information about the toxicity, potency, and elimination rate of the drug, since these properties depend on the overall time spent by the majority of the molecules between the injection location and the delivery location.

We express the channel delay t_{delay} for the path $(n; n = 1 \dots N)$ as

$$t_{\text{delay}} = \frac{1}{T}\int_0^T \arg\max_{t>\tau} h^{(\rho_n,\mu_n;n=1\dots N)}_{(n;n=1\dots N)}(t+\tau,\tau)d\tau \quad (14)$$

where $h^{(\rho_n,\mu_n)}_{(n;n=1\dots N)}(t,\tau)$ is the time-varying impulse response with injection starting at the time τ, and T is the heartbeat period.

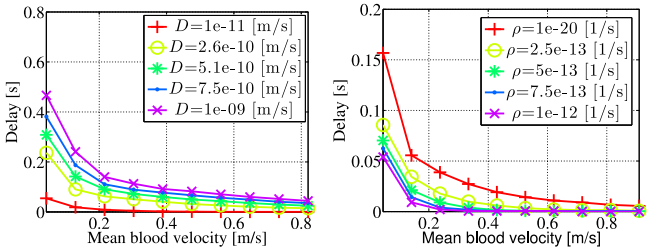

Fig. 6. Effect of the diffusion coefficient D and the absorption rate ρ_n on the channel delay.

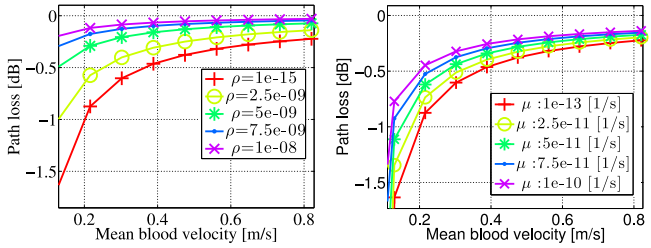

Fig. 7. Effect of the absorption rate (ρ_n) and the reaction rate (μ_n) on the path loss.

Since the channel is time-varying and the blood flow changes periodically, the injected drug particles will be delivered with a different channel delay at the delivery location depending on the blood velocity that was experienced by the body when they were injected. We consider the ambiguity in knowing the blood velocity at the time of injection by averaging over the channel delays for all possible blood velocity values that the body may experience.

The definition of the delay as the average is only acceptable for long propagation times. However, it is acceptable to use the delay as the average value to compare several drug delivery systems that are within the same flow, and propagation length conditions. The standard deviation (or error) in the delay calculation can be highly variable for the scenario where the propagation time is low. If the blood velocity period is higher than the time it takes for the molecules to reach the delivery location, then the error can be as much as in the order of 100%. However, if the blood velocity period is small compared with the delay, then the error is negligible, which means that the injection time is not critical.

B. Channel Path Loss at the Delivery Location

We define the channel path loss for the path $(n; n = 1 \dots N)$ as

$$L = 10 \log_{10} \left(1 - \int_0^{+\infty} h^{(\rho_n, \mu_n; n=1\dots N)}_{(n; n=1\dots N)}(t, 0) dt \right) \quad (15)$$

where $h^{(\rho_n, \mu_n)}_{(n; n=1\dots N)}(t, 0)$ is the time-varying impulse response, which we defined in Section II-B with injection starting at the time $\tau = 0$. This relationship comes from the fact that the impulse response is the probability density of a single particle arriving at a specific location and time. The log-scale is used because about half of the particles are lost at every blood vessel bifurcation, which makes the particle loss follow an exponential trend. In Fig. 6, we see the effect of the blood velocity, the drug diffusion coefficient and the reaction rate on the channel delay. In the numerically evaluated scenario in Fig. 7, we observe that the increase in the drug diffusion coefficient contributes in increasing the delay of the channel, while the effect of the absorption rate contributes in decreasing the delay.

In Fig. 7, we observe that reaction and absorption have similar consequences on the channel path loss. For the absorption, we see that the higher the absorption rate the smaller the delay, which may seem counterintuitive. The reason behind the reduction in delay for increased absorption is that the absorption reduces the number of particles in the blood that are in proximity of the walls, which are the slowest moving particles, thus increasing the average velocity of all the particles.

C. Drug Accumulation in the Rest of the Body

Using the time-varying impulse response, we can calculate the proportions of the drug particles that are either still in the blood, have been absorbed by the surrounding tissues, or have reacted with the blood plasma.

We can express the proportion of drug particles that have been absorbed as follows:

$$d_{\text{absorbed}} = \frac{r_N^2}{r_1^2} \left(\int_0^{+\infty} h^{(0,0;n=1\dots N)}_{(n;n=1\dots N)}(t, 0) dt - \int_0^{+\infty} h^{(0,\mu_n;n=1\dots N)}_{(n;n=1\dots N)}(t, 0) dt \right). \quad (16)$$

Similarly, the proportion of drug particles that have reacted can be expressed as follows:

$$d_{\text{reacted}} = \frac{r_N^2}{r_1^2} \left(\int_0^{+\infty} h^{(0,0;n=1\dots N)}_{(n;n=1\dots N)}(t, 0) dt - \int_0^{+\infty} h^{(0,\mu_n;n=1\dots N)}_{(n;n=1\dots N)}(t, 0) dt \right). \quad (17)$$

Finally, the proportion of drug particles that remain in the blood is equal to the following:

$$d_{\text{blood}} = \frac{r_N^2}{r_1^2} \left(\int_0^{+\infty} h^{(0,0;n=1\dots N)}_{(n;n=1\dots N)}(t, 0) dt \quad (18) - \int_0^{+\infty} h^{(\rho_n,\mu_n;n=1\dots N)}_{(n;n=1\dots N)}(t, 0) dt \right). \quad (19)$$

Therefore, we can use the MC paradigm to predict where the drug is going to accumulate based on the physiological parameters of the drug delivery system and the body. As presented in Fig. 8, the blood vessel conditions cause some variance in the biodistribution. This is moderately important in leaky blood vessels, but is very important in the case of blood vessels affected by arteriosclerosis.

IV. Multiphysics Finite-Element Validation

In order to obtain a pharmacokinetic model of TDDSs, we made the following assumptions: continuous concentration at

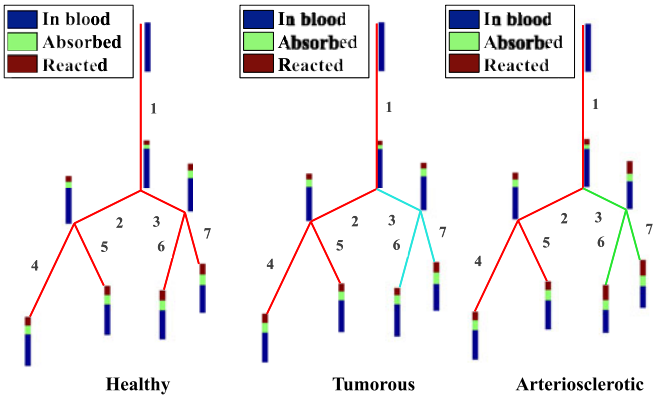

Fig. 8. Effect of cardiovascular diseases on drug distribution.

TABLE I
BLOOD NETWORK BOUNDARY CONDITIONS NUMERICAL VALUES

k	0	1	2	3
$q_{k,1}$	1.3×10^{-4}	2.9×10^{-3}	-1.8×10^{-4}	1.6×10^{-5}
$p_{k,1}$	1.3×10^{-4}	1.7×10^{-4}	5.0×10^{-5}	-6.3×10^{-5}
$q_{k,1}$	1.3×10^{-4}	2.9×10^{-3}	-1.8×10^{-4}	1.6×10^{-5}
$p_{k,2}$	1.3×10^{-4}	1.7×10^{-4}	4.9×10^{-5}	-6.2×10^{-5}
$q_{k,2}$	1.3×10^{-4}	2.8×10^{-3}	-1.7×10^{-4}	1.6×10^{-5}
$p_{k,3}$	7.3×10^{-5}	9.6×10^{-5}	2.8×10^{-5}	-3.5×10^{-5}
$q_{k,3}$	7.3×10^{-5}	1.6×10^{-3}	-9.8×10^{-5}	8.8×10^{-6}
$p_{k,4}$	1.3×10^{-4}	1.7×10^{-4}	4.9×10^{-5}	-6.1×10^{-5}
$q_{k,4}$	1.3×10^{-4}	2.8×10^{-3}	-1.7×10^{-4}	1.5×10^{-5}
$p_{k,5}$	7.2×10^{-5}	9.5×10^{-5}	2.7×10^{-5}	-3.5×10^{-5}
$q_{k,5}$	7.2×10^{-5}	1.6×10^{-3}	-9.6×10^{-5}	8.6×10^{-6}
$p_{k,6}$	7.2×10^{-5}	9.5×10^{-5}	2.7×10^{-5}	-3.5×10^{-5}
$q_{k,6}$	7.2×10^{-5}	1.6×10^{-3}	-9.6×10^{-5}	8.6×10^{-6}
$p_{k,7}$	4.0×10^{-5}	5.3×10^{-5}	1.5×10^{-5}	-1.9×10^{-5}
$q_{k,7}$	4.0×10^{-5}	8.9×10^{-4}	-5.4×10^{-5}	4.9×10^{-6}

the bifurcation, Poiseuille flow, Taylor dispersion approximation, perfectly cylindrical geometry, and infinite-length blood vessels. Using finite-element analysis, the developed model is validated realistically in a 3-D geometry and assuming physical equations in their full forms. In this section, we present the validation of the MC model of TDDSs by simulation using finite-element analysis. We describe the geometry of the simulated system, its governing physical equations, and how the parameters of the analytical model have been mapped to parameters of the finite-element analysis.

Finite element analysis is a numerical method used to solve partial differential equations [9] that underlie the behavior of complex physical systems, including mechanical and chemical transport systems. Finite element analysis has several advantages compared with analytical models. First, finite element analysis allows to simulate objects of arbitrarily complex 3-D geometry. This is especially required for biological objects such as blood vessels which have an imperfectly cylindrical shape and bifurcation shapes. Second, finite element analysis makes it possible to simulate the interaction of different physical phenomena, such as the interaction of the blood vessel walls, the blood flow, which is governed by fluid mechanics, and the chemical transport of drugs. The validation is carried out using COMSOL,[1] a finite element simulation software package.

The following aspects of a drug delivery systems are considered in the simulation as follows:

1) *Blood Flow:* The validation is performed using a 3-D model of a blood arterial network under realistic conditions. The blood flow, which is the main driving force of the drug propagation, is simulated using the 3-D Navier–Stokes equations in the stationary domain. In contrast with existing pharmacokinetic models which are based on unrealistic assumption of having a constant blood flow [19], the drug is propagated through a time-varying blood flow. The blood flow boundary conditions in the arterial networks are estimated based on the realistic transmission line theory which provides results in very good agreement with MRI measurements of blood flow in a human [7].
2) *Geometry:* In the simulation, we assume cylindrically-shaped small blood vessels, which is in agreement with the physiological observations [20]. Large blood vessels and anomalously shaped blood vessels can be considered with little modifications.
3) *Drug Transport:* Through the COMSOL simulation, we observe that the MC model based on Taylor dispersion is a good approximation of particle transport in blood and that, therefore, higher-order approximations [21] which will make the expression of the analytical solution more complex are not needed.
4) *Drug Kinetic Interactions:* The binding is considered by adding a linear reaction term to the 3-D advection-diffusion equation. The absorption is simulated as a boundary condition on the blood vessel walls where the particles are not perfectly bouncing but proportionally lost at the surface. The linear first order kinetics for binding and absorption are common for particles [22]. We assume that no other kind of binding occurs and that particles are at a sufficiently low concentration to avoid nonlinear binding kinetics.

[1]COMSOL is a registered trademarks of COMSOL AB.

A. Topology

For the numerical evaluation of the model, the topology information was derived from the MRI scan of a young male individual, which is available from [17]. However, the available MRI scan anatomical information only covers the large blood vessels. An algorithm that represents the small blood vessels as a fractal tree rooted in the extremity of the large blood vessels was used to obtain the topology of the studied area, in a similar way as in [7]. The numerical values and structure of the topology are listed in this paper and included in Table I to simplify the reproduction of the results. In fact, a blood network was considered, consisting of interconnected blood vessels n, where n is the blood vessel index ($n = 1 \ldots 7$). The *parent blood vessel* 1 bifurcates into two blood vessels, the *daughter blood vessel* 2 and the *daughter blood vessel* 3, and so on. The blood vessel n has a radius r_n and a length l_n, for $n = 1 \ldots 7$. We have

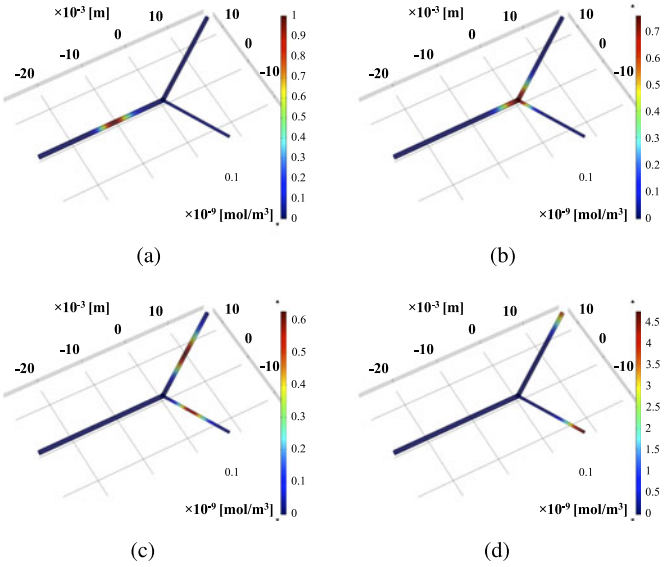

Fig. 9. Evolution of the drug propagation in a tree of blood vessels showing the transport of the injected drug particles from the inlet of the tree of blood vessels to the outlets of the branches, at different times t (a) $t = 46$ ms (b) $t = 92$ ms (c) $t = 138$ ms (d) $t = 184$ ms.

$r_1 = 0.5\,l\text{mm}$, $r_2 = 0.45$ mm, $r_3 = 0.3$ mm, $r_4 = 0.40$ mm, $r_5 = 0.23$ mm, $r_6 = 0.27$ mm, and $r_7 = 0.18$ mm for the radii, and $l_1 = 25$ mm, $l_2 = 22.5$ mm, $l_3 = 15$ mm, $l_4 = 20$ mm, $l_5 = 11.5$ mm, $l_6 = 13.5$ mm, $l_7 = 9$ mm. These dimensions are chosen to be physiologically plausible [17]. According to the physiological data about the size of blood vessels, all types of veins and blood vessels have an interior radius of the blood vessels that is very small compared to the length. This is supported quantitatively in the human and animal physiology literature such as in [17]. In particular, the work in [17] mentions that the length of blood vessels is 25 times the size of their diameters with a standard deviation equal to 5. This study also uses straight cylinders to model blood propagation in blood vessels, which occurs at a faster scale than drug diffusion.

B. Blood Velocity Boundary Conditions

The multiphysics finite-element simulation requires the definition of boundary conditions, which are values defined at the surfaces of the blood network, to find the numerical solutions that satisfy the physical equations. We use five boundary conditions which are defined at the inlet ($n = 1$) and the outlets ($n = 4, 5, 6, 7$) of the blood network as shown in Fig. 9. Thus, there are five boundary conditions which are the *blood velocity* $u_1(t)$ at the inlet of the network, and the blood velocities $u_n(t)$ for the blood vessels n, for $n = 4, 5, 6, 7$, respectively. The numerical values for the boundary conditions have been obtained using the transmission line model developed in [7]. Since the boundary conditions are time-varying and periodic, we express them in terms of their Fourier series decomposition as follows:

$$u_n(t) = \sum_{k=0}^{K-1} p_{k,n} \sin(k\omega_0 t) + q_{k,n} \cos(k\omega_0 t) \tag{20}$$

where $\omega_0 = 2\pi/T$ is the radial sampling frequency, K is the number of samples, and the coefficients $\{p_{k,n}; k = 0 \ldots K-1\}$ and $\{q_{k,n}; k = 0 \ldots K-1\}$ are the even and odd Fourier coefficients, respectively.

C. Drug Propagation Initial Conditions

The drug propagation initial conditions describe the initial values of the drug concentration in the blood network at time t. We express the initial drug concentration $c(x_1, y_1, z_1, t)$ in the blood vessel n as a function of the Cartesian coordinates, with the origin at the center of the inlet of the blood vessel 1, and the $\vec{x}_1$ axis along the longitude of the blood vessel. We approximate the drug injection impulse with a Gaussian function with a very small variance, which we can write as follows:

$$c(x_1, y_1, z_1, t) = \frac{e^{-\frac{x_1^2}{2\sigma_1^2}}}{\sqrt{2\pi\sigma_1^2}} c_0 \tag{21}$$

where x_1 is the Cartesian coordinate along the longitude of the blood vessel 1, σ_1 is the standard deviation of the impulse, and c_0 is the initial concentration of particles. The justification of a drug injection as a Gaussian function rather than a Dirac delta function is essential to obtain the resolution of partial differential equations using using a finite-element methods solver [23].

D. Validation Results

The impulse responses $h^{(\rho_n, \mu_n; n=1\ldots N)}_{(n; n=1\ldots N)}(t, \tau)$ are evaluated at the outlets of the blood vessels n where $n = 1 \ldots 3$. We evaluate the impulse response $h^{(\rho_n, \mu_n)}_{(n)}(t, \tau)$ as

$$h^{(\rho_n, \mu_n; n=1\ldots N)}_{(n; n=1\ldots N)}(t, \tau) = \frac{1}{S_{O_n}} \int_{M(x,y,z_n) \in O_n} c(x, y, z_n, t) dx dy dz \tag{22}$$

where O_n denotes the outlet of the blood vessel n, S_{O_n} is the surface area of O_n, $M(x, y, z_n)$ is a point in O_n, and $c(x, y, z_n, t)$ is the concentration at the time instant t and the point with the coordinates (x, y, z_n).

The simulations were performed using COMSOL on a desktop machine with a total computation time of 2 h 57 min to build the map of blood velocity and for the propagation of drug particles, for a simulation duration $T_{\text{sim}} = 0.25$ s. Table I lists the Fourier coefficients that have been used in the multiphysics finite-element calculations.

In Fig. 10, we compare the impulse responses obtained by multiphysics finite-element simulation with the analytical results obtained using the MC model described in Section II, where we use the following values for the diffusion coefficient $D = 10^{-8}\text{m}^2/\text{s}$ and the absorption rates ($\rho_n = 1e-5; n = 1 \ldots 7$). We compare the results for all three blood vessels 1, 4, and 5, and we notice in the three cases that there is good agreement between the values generated through the simulation and the model.

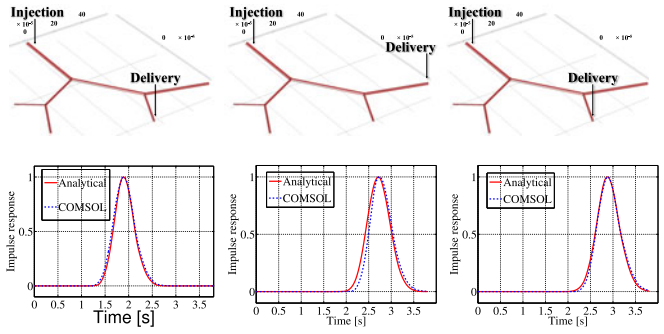

Fig. 10. Comparison between the impulse responses obtained by the MC model and the impulse responses obtained by the multiphysics finite-element simulation technique for different delivery locations at the outlet of the blood vessels 1, 4, and 5, respectively.

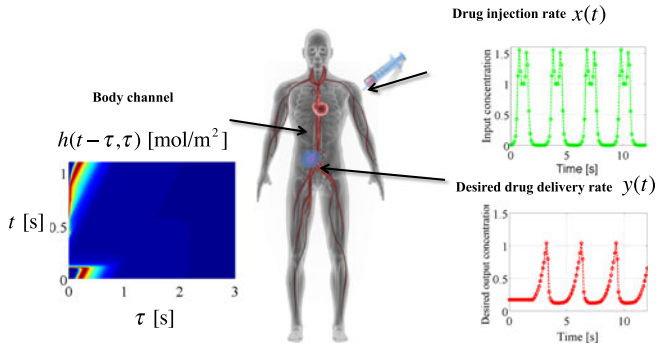

Fig. 11. Scheme of the injection rate rate optimization for a desired drug delivery rate.

V. Drug Injection Optimization

In this section, we aim to propose a solution to the optimization of the drug injection in order to achieve a desired drug delivery rate, based on the MC-based pharmacokinetic model presented in Section II. In order to obtain efficient drug delivery systems, the timing and location of the drug particles are crucial. The diseased region needs to receive the particles at the right time and in the right quantity. When the particles are injected by systemic administration, the drug particles can be lost in blood vessel bifurcations, absorbed by blood vessels, and mixed with the blood due to diffusion. Fig. 11 shows a scheme of the injection rate optimization, where, starting from the desired delivery rate, an optimal injection rate is found giving exactly the desired delivery rate with minimal error.

In the following, we present a method to find the optimal inject rate based on the desired drug delivery rate, the physiological parameters of the body, the drug properties, the injection location and the delivery location.

We consider a disease that requires a specific drug delivery rate that will make the healing effective, with just a minimal number of drug particles, and below the level that causes toxicity. We suppose that a desired drug injection rate is given by a time-varying function $x(t)$, which describes the drug concentration rate at every time t in the injection location.

Using the pharmacokinetic model in Section II, we obtain a channel model characterized by a time-varying impulse response $h_{(n;n=1\ldots N)}^{(\rho_n,\mu_n;n=1\ldots N)}(t,\tau)$ which relates the drug injection rate $x(t)$ to the drug delivery rate $y(t)$, by the following relationship:

$$y(t) = \int_{-\infty}^{+\infty} h_{(n;n=1\ldots N)}^{(\rho_n,\mu_n;n=1\ldots N)}(t,\tau)x(\tau)d\tau\,. \tag{23}$$

Here, our objective is to find the optimal drug injection rate $x^*(t)$, such that the obtained drug delivery rate $y^*(t)$ is as close as possible to the drug delivery rate $y(t)$. This is expressed by

$$x^*(t) = \arg\min_{x(t)} \|y(t) - y^*(t)\|\,. \tag{24}$$

Using the time-varying impulse response, the previous expression becomes

$$x^*(t) = \arg\min_{x(t)} \left\| \int_{-\infty}^{+\infty} h_{(n;n=1\ldots N)}^{(\rho_n,\mu_n;n=1\ldots N)}(t,\tau)x(\tau)d\tau - y^*(t) \right\| \tag{25}$$

where $h_{(n;n=1\ldots N)}^{(\rho_n,\mu_n;n=1\ldots N)}(t,\tau)$ is the time-varying impulse response that characterizes the drug propagation from the injection location to the delivery location.

y_j is defined as follows:

$$y_j = \int_0^{jT_s} h_{(n;n=1\ldots N)}^{(\rho_n,\mu_n;n=1\ldots N)}(t_j,\tau)x(\tau)d\tau\,. \tag{26}$$

x_i is defined as

$$x_i = x(iT_s) \tag{27}$$

where $i,j = 1\ldots K$, K is the number of samples, and T_s is the sampling period. With this notation, we can write

$$y_j = \sum_{i=1}^{j} x_i \int_{(i-1)T_s}^{iT_s} h_{(n;n=1\ldots N)}^{(\rho_n,\mu_n;n=1\ldots N)}(jT_s,\tau)d\tau\,. \tag{28}$$

We define the channel coefficients $h_{i,j}^{(\rho_n,\mu_n;n=1\ldots N)}$ as follows:

$$h_{i,j}^{(\rho_n,\mu_n;n=1\ldots N)} = \int_{(i-1)T_s}^{iT_s} h_{(n;n=1\ldots N)}^{(\rho_n,\mu_n;n=1\ldots N)}(t_i,\tau)d\tau\,. \tag{29}$$

Therefore, we get the following expression:

$$y_j = \sum_{i=1}^{j} x_i h_{i,j}^{(\rho_n,\mu_n;n=1\ldots N)}\,. \tag{30}$$

Thus, the problem can be written in matrix notation as

$$\underline{y} = \mathbf{H}_{(n;n=1\ldots N)}^{(\rho_n,\mu_n;n=1\ldots N)}\underline{\mathbf{x}} \tag{31}$$

where $\underline{y} = [y_j; j = 1\ldots K]'$ is a K-dimensional vector whose elements are samples of the desired delivery rate, $\underline{x} = [x_i; i = 1\ldots K]'$ is a K-dimensional vector whose elements are samples of the optimal injection rate, and $\mathbf{H}_{(n;n=1\ldots N)}^{(\rho_n,\mu_n;n=1\ldots N)}$ is the square matrix of size K-by-K, whose components are defined in (29), and $[.]'$ is the vector transpose operator.

The matrix $\mathbf{H}_{(n;n=1\ldots N)}^{(\rho_n,\mu_n;n=1\ldots N)}$ is supposed to be invertible. In case the matrix is not invertible, the linear matrix inequality approach as proposed in [24] can be directly adapted to the MC model to find the optimal injection rate.

We define the vector $\underline{x}^* = [x_i; i = 1 \dots K]'$ as follows:

$$\underline{x}^* = \left\{ \mathbf{H}^{(\rho_n, \mu_n; n=1 \dots N)}_{(n; n=1 \dots N)} \right\}^{-1} \underline{\mathbf{y}} \tag{32}$$

where $\left\{ \mathbf{H}^{(\rho_n, \mu_n; n=1 \dots N)}_{(n; n=1 \dots N)} \right\}^{-1}$ is the inverse of the matrix $\mathbf{H}^{(\rho_n, \mu_n; n=1 \dots N)}_{(n; n=1 \dots N)}$.

The desired drug injection rate is found by

$$x^*(t) = \sum_{i=1}^{i=K} x_i^* \cdot \operatorname{sinc}\left(\frac{t - iT_s}{T_s} \right). \tag{33}$$

According to the Nyquist criterion [25], the sampling period should satisfy $T_s < \frac{1}{2B}$, where B is the bandwidth of the time-varying impulse response of the system. The sampling period depends on the blood velocity and the characteristic time scale of the advection-diffusion. For the simulations, a value of $T_s = 15.645$ ms, which is the sampling period of the measured blood cardiac flow input was chosen. This is much shorter than the characteristic time scale of the advection-diffusion.

VI. Conclusion

In this paper, we propose to apply the abstraction of the MC paradigm to address important problems in TDDSs, namely, modeling the drug pharmacokinetics, estimating the biodistribution, and optimizing the drug injection rate. The MC abstraction allowed to obtain an analytical pharmacokinetic model that accounts for various physicochemical processes in the particle propagation, and takes into account the impact of cardiovascular diseases. By stemming from the pharmacokinetic model, we proposed to use communication engineering metrics to estimate the drug biodistribution at the delivery location, while analytical expressions are obtained to estimate the drug accumulation in the rest of the body. We have favorably compared our pharmacokinetic model with multiphysics finite-element simulations of the drug propagation in the arterial system, and provided numerical results for the drug biodistribution in different scenarios. We also proposed a procedure to optimize the drug injection rate according to a desired drug delivery rate through the pharmacokinetic model when the injection location and delivery are known.

The pharmacokinetic model presented in this paper does not take into account particles that continue their propagation after having circulated the entire cardiovascular system. This is justified by the fact that heart and veins tend to significantly disperse the particles, therefore favoring their accumulation over their recirculation in the cardiovascular system. A possible future extension of this study could also include these effects in the pharmacokinetics through a stochastic model derived from an MC noise abstraction, as presented in [26].

The results presented in this paper can support the future design of intrabody MC networks [27]. In fact, the developed pharmacokinetic model has the potential to be used to predict the propagation of MC signals in the human body undergoing several transport and kinetic processes. With regards to the communication performance of such a system, the theoretical limits of the amount information that can be reliably transmitted by MC over the blood vessels has been studied in [26]. By defining the encoding and modulation schemes for MC in the cardiovascular system, the achievable bit error rates can be evaluated.

In conclusion, the proposed abstraction of a TDDS with the MC paradigm provides a new way to model the TDDSs and support their engineering with tractable, yet complete, analytical models.

References

[1] M. N. V. R. Kumar, *Handbook of Particulate Drug Delivery*. CA, USA: American Scientific Publishers, 2011.

[2] A. M. Alkilany *et al.*, "Gold nanorods: Their potential for photothermal therapeutics and drug delivery, tempered by the complexity of their biological interactions," *Adv. Drug Del. Rev.*, vol. 64, no. 2, pp. 190–199, 2012.

[3] S. Willmann *et al.*, "Development of a physiology-based whole-body population model for assessing the influence of individual variability on the pharmacokinetics of drugs," *J. Pharmacokinetics Pharmacodynamics*, vol. 34, no. 3, pp. 401–431, 2007.

[4] M. Dostalek *et al.*, "Pharmacokinetics, pharmacodynamics and physiologically-based pharmacokinetic modelling of monoclonal antibodies," *Clin. Pharmacokinetics*, vol. 52, no. 2, pp. 83–124, 2013.

[5] P. D. Marcato, "Pharmacokinetics and pharmacodynamics of nanomaterials," in *Nanotoxicology*. New York, NY, USA: Springer, 2014, pp. 97–110.

[6] D. Li *et al.*, "Using a pbpk model to study the influence of different characteristics of nanoparticles on their biodistribution," *J. Phys.: Conf. Series*, vol. 429, no. 1, pp. 012019-1–012019-7, 2013.

[7] Y. Chahibi *et al.*, "A molecular communication system model for particulate drug delivery systems," *IEEE Trans. Biomed. Eng.*, vol. 60, no. 12, pp. 3468–3483, Dec. 2013.

[8] C. *et al.*, "Delivery of molecular and nanoscale medicine to tumors: Transport barriers and strategies," *Annu. Rev. Chem. Biomolecular Eng.*, vol. 2, pp. 281–298, 2011.

[9] K. Avgoustakis *et al.*, "Plga–mpeg nanoparticles of cisplatin: In vitro nanoparticle degradation, in vitro drug release and in vivo drug residence in blood properties," *J. Controlled Release*, vol. 79, no. 1, pp. 123–135, 2002.

[10] C. D. Walkey *et al.*, "Nanoparticle size and surface chemistry determine serum protein adsorption and macrophage uptake," *J. Amer. Chem. Soc.*, vol. 134, no. 4, pp. 2139–2147, 2012.

[11] R. R. Biswas and P. N. Sen, "Taylor dispersion with absorbing boundaries: A stochastic approach," *Phys. Rev. Lett.*, vol. 98, no. 16, pp. 164501-1–164501-4, 2007.

[12] M. Levesque *et al.*, "Taylor dispersion with adsorption and desorption," *Phys. Rev. E*, vol. 86, no. 3, pp. 036316-1–036316-5, 2012.

[13] P. Vanassche *et al.*, "Symbolic modeling of periodically time-varying systems using harmonic transfer matrices," *IEEE Trans. Comput.-Aided Design Integr. Circuits Syst.*, vol. 21, no. 9, pp. 1011–1024, Sep. 2002.

[14] G. McVeigh *et al.*, "Evaluation of mechanical arterial properties: Clinical, experimental and therapeutic aspects," *Clin. Sci.*, vol. 102, pp. 51–67, 2002.

[15] B. Syeda *et al.*, "Arterial compliance: A diagnostic marker for atherosclerotic plaque burden?," *Amer. J. Hypertension*, vol. 16, no. 5, pp. 356–362, 2003.

[16] J. Ottesen *et al.*, *Applied Mathematical Models in Human Physiology*. Philadelphia, PA, USA: SIAM, 2004.

[17] M. S. Olufsen *et al.*, "Numerical simulation and experimental validation of blood flow in arteries with structured-tree outflow conditions," *Ann. Biomed. Eng.*, vol. 28, no. 11, pp. 1281–1299, 2000.

[18] J. DiPiro *et al.*, *Concepts in Clinical Pharmacokinetics*. MD, USA: Amer. Soc. Health-Syst. Pharmacists, 2010.

[19] F. Gentile *et al.*, "The transport of nanoparticles in blood vessels: The effect of vessel permeability and blood rheology," *Ann. Biomed. Eng.*, vol. 36, no. 2, pp. 254–261, 2008.

[20] J. Ottesen *et al.*, *Applied Mathematical Models in Human Physiology*. Philadelphia, PA, USA: SIAM, 2004.

[21] V. Balakotaiah and H.-C. Chang, "Dispersion of chemical solutes in chromatographs and reactors," *Philos. Trans. Roy. Soc. London Series A: Phys. Eng. Sci.*, vol. 351, no. 1695, pp. 39–75, 1995.

[22] G. A. Hughes, "Nanostructure-mediated drug delivery," *Nanomed.: Nanotechnol., Biol. Med.*, vol. 1, no. 1, pp. 22–30, 2005.
[23] B. H. Devkota and J. Imberger, "Lagrangian modeling of advection-diffusion transport in open channel flow," *Water Resources Res.*, vol. 45, no. 12, pp. W12406-1–W12406-14 2009.
[24] S. Wang *et al.*, "H 2 optimal inverse of periodic fir digital filters," *IEEE Trans. Signal Process.*, vol. 48, no. 9, pp. 2696–2700, Sep. 2000.
[25] L. A. Zadeh and C. A. Deoser, *Linear System Theory*. Melbourne, FL, USA: Krieger, 1976.
[26] Y. Chahibi and I. Akyildiz, "Molecular communication noise and capacity analysis for particulate drug delivery systems," *IEEE Trans. Commun.*, vol. 62, no. 11, pp. 3891–3903, Nov. 2014.
[27] I. F. Akyildiz *et al.*, "Internet of bionanothings," *IEEE Commun. Mag.*, vol. 53, no. 3, pp. 32–40, Mar. 2015.

Youssef Chahibi (S'13) received the Diplôme d'Ingénieur in telecommunications and networks from Institut National Polytechnique de Toulouse, Toulouse, France, in 2011, and the M.S. degree from the Georgia Institute of Technology, Atlanta, GA, USA, in 2012.

During 2011, he was a Physical-Layer Engineer at Alcatel-Lucent, Antwerp, Belgium. In the summer of 2014, he was a Guest Research Scholar at the Nano Communication Center, Tampere University of Technology, and during 2015, he was a Fellow of the Research Council of Norway, Norwegian University of Science and Technology, Trondheim, Norway. His research interests are in nanoscale biologically-inspired communications and drug delivery systems.

Massimiliano Pierobon (M'05) received the M.S. degree in telecommunication engineering from the Politecnico di Milano, Milan, Italy, in 2005, and the Ph.D. degree in electrical and computer engineering from the Georgia Institute of Technology, Atlanta, GA, USA, in 2013.

He is currently an Assistant Professor at the Department of Computer Science and Engineering, University of Nebraska-Lincoln, Lincoln, NE, USA. He received the BWN Lab Researcher of the Year Award at the Georgia Institute of Technology for his outstanding research achievements in 2011. He was also named IEEE Communications Letters 2013 Exemplary Reviewer in appreciation for his service as referee. He is an Editor of the IEEE TRANSACTIONS IN COMMUNICATIONS. He is a Member of ACM and ACS. His current research interests are in molecular communication theory for nanonetworks, communication engineering applied to intelligent drug delivery systems, and telecommunication engineering applied to cell-to-cell communications.

Ian F. Akyildiz (M'86–SM'89–F'96) received the B.S., M.S., and Ph.D. degrees in computer engineering from the University of Erlangen-Nurnberg, Erlangen, Germany, in 1978, 1981, and 1984, respectively.

He is currently the Ken Byers Chair Professor in telecommunications at the School of Electrical and Computer Engineering, Georgia Institute of Technology, Atlanta, GA, USA, the Director of the Broadband Wireless Networking Laboratory and Chair of the Telecommunication Group, Georgia Tech. He is an Honorary Professor at the School of Electrical Engineering, Universitat Politecnica de Catalunya, Barcelona, Spain, and the Founder of N3Cat (NaNoNetworking Center in Catalunya). He is also an Honorary Professor at the Department of Electrical, Electronic and Computer Engineering, University of Pretoria, Pretoria, South Africa, and the Founder of the Advanced Sensor Networks Lab. Since 2011, he has been a Consulting Chair Professor at the Department of Information Technology, King Abdulaziz University, Jeddah, Saudi Arabia. Since January 2013, he is also a FiDiPro Professor (Finland Distinguished Professor Program supported by the Academy of Finland) at the Department of Communications Engineering, Tampere University of Technology, Tampere, Finland. He is the Editor-in-Chief of *Computer Networks* (Elsevier), and the founding Editor-in-Chief of the *Ad Hoc Networks* (Elsevier), *Physical Communication* (Elsevier), and the *Nano Communication Networks* (Elsevier). He is an ACM Fellow. He has received numerous awards from IEEE and ACM. According to Google Scholar, as of May 2014, his h-index is 90 and the total number of citations he received is 70+K. His current research interests are in molecular communication, nano-scale machine communication, 5G cellular systems, software-defined networking, and underground wireless sensor networks.